REGULAR PAPER

Electric field-induced change in the crystal structure of MOCVD-Pb(Zr,Ti)O_3 films near the phase boundary

To cite this article: Hidehisa Inoue *et al* 2019 *Jpn. J. Appl. Phys.* **58** SLLB07

Japanese Journal of Applied Physics **58**, SLLB07 (2019) **REGULAR PAPER**
https://doi.org/**10.7567/1347-4065/ab37ef**

Electric field-induced change in the crystal structure of MOCVD-Pb(Zr,Ti)O_3 films near the phase boundary

Hidehisa Inoue, Takao Shimizu, and Hiroshi Funakubo*

School of Materials and Chemical Technology, Tokyo Institute of Technology, Yokohama 226-8502, Japan

*E-mail: funakubo.h.aa@m.titech.ac.jp

Received June 7, 2019; revised June 29, 2019; accepted July 31, 2019; published online August 22, 2019

The change in the crystal structure after poling and under an constant electric field was investigated for Pb(Zr_xTi_{1-x})O_3 films. The preparation of approximately 1.5 μm thick $(100)_T/(001)_T/(100)_R$-oriented Pb(Zr_xTi_{1-x})O_3 films with a Zr/(Zr + Ti) ratio of 0.54–0.67 took place on $(100)_C$$SrRuO_3$/(100) $_C$$LaNiO_3$/(111)Pt/$TiO_2$/$SiO_2$/Si substrates by pulsed metal organic chemical vapor deposition. Increasing Zr/(Zr + Ti) ratio provides a change in the constituent phases of the films from single-phase tetragonal to a mixture of tetragonal and rhombohedral phases, and finally, to single-phase rhombohedral. The crystal structure of all films changed after the poling process and under an electric field in various ways according to the Zr/(Zr + Ti) ratios of the films; including lattice elongation, domain switching, and phase change. In particular, a single peak from the rhombohedral phase is asymmetrically broadened by both the poling process and an applied electric field suggesting that a (100)-oriented rhombohedral phase presumably changed to a (001)-oriented tetragonal phase. © 2019 The Japan Society of Applied Physics

1. Introduction

Because of their high dielectric constant and large piezoelectricity, ferroelectrics have been investigated and are widely used in various electronic devices.[1–4] In recent years, with the development of micro-electro-mechanical system technology, ferroelectric materials have been used for thin film applications, such as thin film sensors and thin film actuators.[5,6] Among the ferroelectric materials, a solid solution of $PbTiO_3$ and $PbZrO_3$, Pb(Zr_xTi_{1-x})O_3 (PZT), is the most widely used because of its large piezoelectricity for a Zr/(Zr + Ti) ratio near the phase boundary between the tetragonal phase of the $PbTiO_3$-rich composition and rhombohedral phase of the $PbZrO_3$-rich composition, the so-called morphotropic phase boundary (MPB).[7–9]

There are many reports clarifying the origin of the large piezoelectric response, in both bulk[10,11] and film samples,[12–14] especially from the viewpoint of crystal structure. Most studies on PZT discuss the relationship between the crystal structure of as-deposited films and the piezoelectric responses.[15–17] Nevertheless, a poling treatment was usually required to activate the piezoelectric properties. It is well recognized that the poling treatment often changes the crystal structure of ferroelectric materials based on the studies of the bulk samples.[18,19] Hence, the relationship between the piezoelectric response after poling and the crystal structure is essential, although few studies to clarify the relationship have been performed with film samples. In addition, it is also important to investigate the change in the crystal structure under an electric field because the piezoelectric response is considered to accompany the crystal structural change under the application of an electric field.

Kovacova et al. reported the phase transformation from (100)-oriented tetragonal to (100)-oriented rhombohedral phases under an electric field for a PZT film of 1 μm thickness, consisting of a mixture of tetragonal and rhombohedral phases.[19] However, there was no switching from the (100) to (001) orientation of the tetragonal phase in that study, even though other studies have reported the presence of this switching for pure tetragonal films.[14,20,21] Domain switching to the (001)-oriented tetragonal domain is considered to be plausible, even from the rhombohedral domain, because the polarization direction is parallel to the surface normal direction, along which an electric field is applied. This has been pointed out for some single crystals of Pb-based relaxor ferroelectrics from both experimental and theoretical viewpoints.[22,23] Therefore, it is an interesting question whether such a domain rotation occurs after poling and under an electric field near the MPB. However, such a change by an electric field has been scarcely reported for various Zr/(Zr + Ti) ratios near the phase boundary.

Herein, we investigated the change in the crystal structure after the poling process and under an electrical field using a microbeam X-ray diffraction (XRD) study for $(100)_T/(001)_T/(100)_R$-oriented PZT films with a thickness of 1.5 μm near the MPB composition, where $(100)_T$, $(001)_T$, and $(100)_R$ refer to the (100) orientation of the tetragonal phase, (001) orientation of the tetragonal phase, and (100) orientation of the rhombohedral phase, respectively. The crystal structures changed in different ways according to their compositions. These results suggest a change from the (100)-oriented rhombohedral phase to the (001)-oriented tetragonal phase, as well as switching from the tetragonal (100) to (001) orientation, not only after the poling process but also under the application of an electric field.

2. Experimental procedure

Pb(Zr_xTi_{1-x})O_3 films with the Zr/(Zr + Ti) ratio of 0.54–0.67 were deposited at 700 °C by pulsed metal organic chemical vapor deposition. $Pb(C_{11}H_{19}O_2)_2$, $Zr(O{\cdot}t\text{-}C_4H_9)_4$, and $Ti(O{\cdot}i\text{-}C_3H_7)_4$ were used as the source materials of Pb, Zr, and Ti, respectively. The thickness of the films was approximately 1.5 μm. Nitrogen and oxygen gases were used as a carrier gas of these source materials and as an oxidant gas, respectively. The chamber pressure during the deposition was maintained at 670 Pa. Details of the deposition are already reported elsewhere.[24,25] The Zr/(Zr + Ti) ratio of the films was changed by controlling the input Zr to Ti concentration ratio from the source materials, while maintaining a constant Pb/(Pb + Zr + Ti) ratio at 0.5 as shown in Fig. 1, where $R[Zr(O{\cdot}t\text{-}C_4H_9)_4]$ and $R[Ti(O{\cdot}i\text{-}C_3H_7)_4]$ are the theoretical flow rates of the Zr and Ti source gases.[24,25] The theoretical flow rate (R) is defined by the vapor pressure for the source

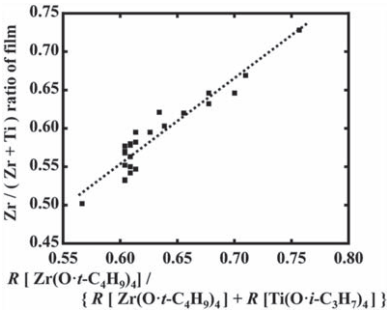

Fig. 1. Zr/(Zr + Ti) ratio of the films as a function of R[Zr(O·t-C_4H_9)$_4$]/{R [Zr(O·t-C_4H_9)$_4$] + R[Ti(O·t-C_3H_7)$_4$]}. R[Zr(O·t-C_4H_9)$_4$] and R[Ti(O·i-C_3H_7)$_4$] are the theoretical flow rates of the Zr and Ti source gases, respectively.

materials at the temperature of vaporizer [$P(T_v)$], the pressure of vaporizer (P_v) and the carrier gas flow rate (l) as follows

$$R = \frac{P(T_v)}{P_v} l. \quad (1)$$

The film thickness was adjusted by the deposition time. The $SrRuO_3$ film was used as a conductive bottom electrode layer on account of its good lattice matching with $Pb(Zr_xTi_{1-x})O_3$ film and its high conductivity. To grow $(100)_T/(001)_T/(100)_R$-oriented $Pb(Zr_xTi_{1-x})O_3$ films, the $(100)_C$-oriented $SrRuO_3$ bottom electrode layer was prepared by inserting the $LaNiO_3$ buffer layer; the resultant stacking of substrate was $(100)_C SrRuO_3/(100)_C LaNiO_3/(111)Pt/TiO_2/SiO_2/Si$.[26] The pseudo-cubic Miller index was used for $SrRuO_3$ and $LaNiO_3$, and is denoted as $(hkl)_C$ in the present study. All buffer layers and electrodes were deposited by the RF magnetron sputtering method.

The film composition was characterized by X-ray fluorescence spectrometry (PANalytical, PW4400) using standard samples. The crystal structure and orientation of the films were analyzed by X-ray diffractometer (PANalytical, X'part MRD) with Cu-$K\alpha$ radiation. Electric properties were measured using a ferroelectric tester (Toyo Corp. FCE-1). Pt top electrodes with 200 μm φ were deposited onto PZT films by evaporation for the measurement of ferroelectric properties. Micro-area XRD set up with a 2D detector (Bruker AXS D8 DISCOVER) was used to evaluate the crystal structure of the films before, after, and under application of an electric field by focusing an X-ray on Pt top electrodes.[27]

3. Results and discussion

Figure 2 shows the XRD patterns of $Pb(Zr_xTi_{1-x})O_3$ films with various Zr/(Zr + Ti) ratios. All patterns showed only PZT $h00_T/00l_T/h00_R$ diffraction peaks. This indicates a $(100)_T/(001)_T/(100)_R$-orientation of the films, irrespective of the film Zr/(Zr + Ti) ratio. The inset figure shows the X-ray pole figure data measured at the 2θ angle, corresponding to PZT {110} diffraction peak, revealing a ring-shaped pattern located at an inclination angle Ψ of approximately 45°. This result means that $(100)_T/(001)_T/(100)_R$-oriented $Pb(Zr_xTi_{1-x})O_3$ films with an in-plane random orientation were grown onto $(100)_c SrRuO_3/(100)_c LaNiO_3/(111)Pt/TiO_2/SiO_2/Si$ substrates.

Figure 3 shows enlarged XRD patterns for $2\theta = 94°$–$104°$ for the as-deposited films. The pattern for the film with Zr/(Zr + Ti) = 0.54 shows a clear split, forming two peaks assigned to the 004 and 400 reflections from the tetragonal

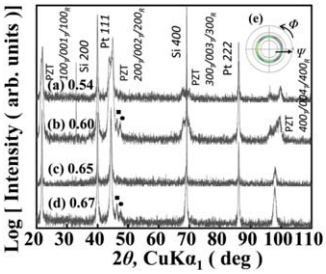

Fig. 2. (Color online) (a)–(d) X-ray diffraction (XRD) patterns of $Pb(Zr_xTi_{1-x})O_3$ films with Zr/(Zr + Ti) ratios of (a) 0.54, (b) 0.62, (c) 0.65, and (d) 0.67. (e) X-ray pole figure data measured at 2θ angle corresponding to the PZT {110} diffraction peak for the $Pb(Zr_xTi_{1-x})O_3$ films with a Zr/(Zr + Ti) ratio of 0.54. Symbols of filled circles and filled squares indicate the peaks from $SrRuO_3$ and $LaNiO_3$, respectively.

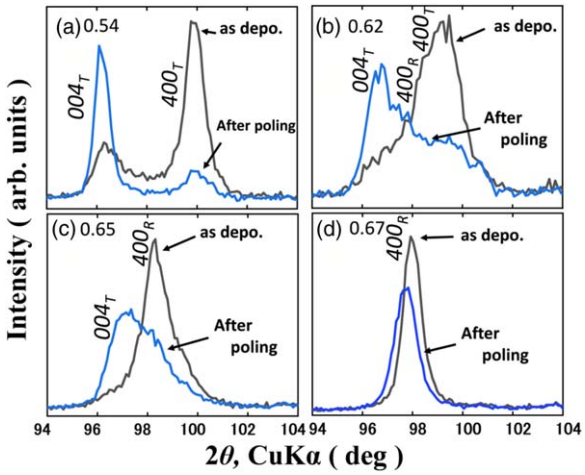

Fig. 3. (Color online) XRD patterns of $Pb(Zr_xTi_{1-x})O_3$ films with Zr/(Zr + Ti) ratios of (a) 0.54, (b) 0.62, (c) 0.65, and (d) 0.67 for as-deposited films (black line) and after the poling process of up to approximately 260 kV cm^{-1} (blue line).

phase, while films with Zr/(Zr + Ti) = 0.65 and 0.67 show only one peak attributed to the 400 reflection from the rhombohedral phase. There are three peaks in the pattern for the film with Zr/(Zr + Ti) = 0.62, i.e. the 400 and 004 peaks of the tetragonal phase located at the highest and lowest angles, respectively, and the 400 peak from the rhombohedral phase located at the middle angle. These results suggest that the film with Zr/(Zr + Ti) = 0.54 consists of the tetragonal single-phase with (100)/(001) orientation, while the films with Zr/(Zr + Ti) = 0.65 and 0.67 consist of the rhombohedral single-phase with (100) orientation. The film with Zr/(Zr + Ti) = 0.60 is considered to be the mixture of tetragonal and rhombohedral phases with (100)/(001) and (100) orientations, respectively.

Figure 4 shows the polarization-electric field relationships measured by applying an electric field of approximately 260 kV cm^{-1} to the films, shown in Figs. 2 and 3. Well-saturated hysteresis loops originating from the ferroelectricity were observed for all films. The remnant polarization (P_r) value was almost the same, irrespective of the Zr/(Zr + Ti) ratio in the present Zr/(Zr + Ti) ratio range, as our previous study indicated.[28] This shows that the P_r value was almost independent of the constituent phase of the as-deposited films. On the other hand, the coercive field monotonously

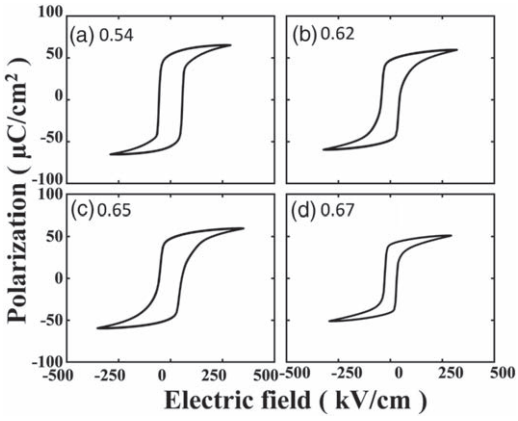

Fig. 4. Polarization-electric field relationships measured under an electric field up to approximately 260 kV cm^{-1} for the same films shown in Figs. 2 and 3.

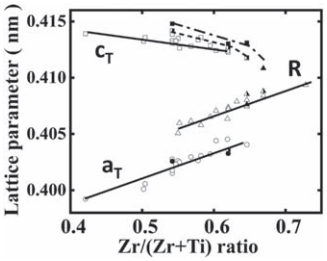

Fig. 5. Lattice parameters as a function of the Zr/(Zr + Ti) ratio for the as-deposited films (open symbols and solid lines) and films after the poling process up to approximately 260 kV cm^{-1} (half-closed symbols and dotted line) and under the application of an electric field (closed symbols and dashed and dotted line). Open and square symbols, respectively, show the a-axis (a_T) and c-axis (c_T) of the tetragonal phase, while triangle symbols show the a-axis (a_R) of the rhombohedral phase.

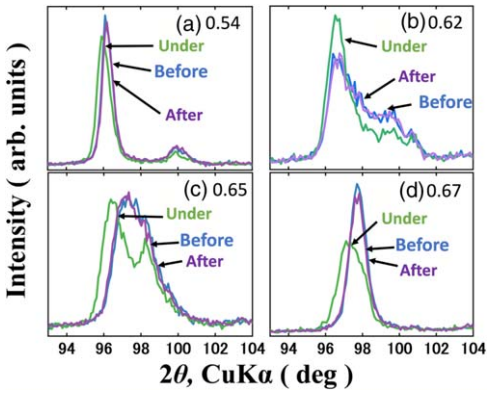

Fig. 6. (Color online) XRD patterns of Pb(Zr_xTi_{1-x})O_3 films with Zr/(Zr + Ti) ratios of (a) 0.54, (b) 0.62, (c) 0.65, and (d) 0.67 for before (corresponding to after poling) (purple line), under (green line), and after (blue line) application of an electric field of approximately 260 kV cm^{-1}.

decreased with increasing Zr/(Zr + Ti) ratio, which is also the same trend as the previous reports.[28,29)]

Figure 3 also displays the XRD patterns of the films after the poling process by an electric field of 260 kV cm^{-1}. In the case of Zr/(Zr + Ti) = 0.54, shown in Fig. 3(a), intensities of tetragonal 004 and 400 peaks increased and decreased, respectively, after the poling process. This means that the domain switching occurred from the (100) to (001) orientation of the tetragonal phase by the poling process, corresponding with our previous reports for 2 μm thick films with Zr/(Zr + Ti) ratios of 0.39 and 0.5.[30)] Kungl et al. also reported similar results.[21)] Note that the peak position of tetragonal 004 shifted to a lower angle by the poling process. This suggests an increase in the c-axis lattice parameter of the tetragonal phase. The films with Zr/(Zr + Ti) = 0.62 exhibited a change in the film similar to that with Zr/(Zr + Ti) = 0.54, shown in Fig. 3(a), despite the existence of the rhombohedral domain. For the film with a Zr/(Zr + Ti) ratio of 0.65, the peak became asymmetrically broader by the poling process, and the peak position of the rhombohedral 400 diffraction seemed to shift to a lower angle. The peak broadening possibly suggests the generation of the tetragonal phase by the poling process; namely, some of the rhombohedral domains were transformed to (001)-oriented tetragonal domains. Unlike these compositions, a single peak of rhombohedral 400 remained, and the peak shifted to a lower angle by the poling process for Zr/(Zr + Ti) = 0.67, as shown in Fig. 3(d). It must be noted that the sum of the peak area after poling treatment decreased compared with the as-deposited film. This likely originated from the change in the structural factor among the different orientations. The change in the ionic position possibly occurred, which also varied the structural factors.

To analyze the crystal structural change by the poling process shown in Fig. 3, lattice parameters are plotted in Fig. 5 as functions of the Zr/(Zr + Ti) ratio for the as-deposited films and films after the poling process with an electric field of approximately 260 kV cm^{-1}. For the as-deposited films, the tetragonal phase was detected up to the Zr/(Zr + Ti) ratio of 0.62, while the rhombohedral phase was confirmed down to 0.55, as shown in Fig. 3. As a result, single-phase tetragonal and rhombohedral phases were obtained for the films with a Zr/(Zr + Ti) ratio below 0.55 and above 0.62, respectively, and the mixture of these two was done between ratios of 0.55 and 0.62.

The lattice parameters after the poling process are plotted as half-closed symbols in Fig. 5. The c-axis lattice parameter of the tetragonal phase is found to increase by the poling process. The lattice parameter corresponding to the lower angle peak for the film with Zr/(Zr + Ti) = 0.65 lies on the extrapolated line of the c-axis lattice parameter of the tetragonal phase after the poling process (dashed line in Fig. 6), indicating the existence of the (001)-oriented domain. This suggests a partial phase change from the (100)-oriented rhombohedral phase to (001)-oriented tetragonal phase, and the phase change caused the peak broadening in Fig. 3(c), which implies the existence of two peaks.

To discuss the field-induced strain, the XRD measurements were also performed under the application of an electric field. Figure 6 shows XRD patterns of before, after, and under an electric field of about 260 kV cm^{-1} for the same films shown in Figs. 2–5. Note that the data before the application of the electric field correspond to the data after the poling process shown in Fig. 3. The XRD patterns measured under the electric field dramatically changed from those before the electric field application, suggesting that the crystal structure changed under the electric field. It should be mentioned that the XRD patterns measured before and after application were the same for all films, indicating that the overserved change in the crystal structure under the electric

field was reversible, and the crystal structure relaxed into the original structure after the removal of the electric field for all films.

For the film with a Zr/(Zr + Ti) ratio of 0.54, shown in Fig. 6(a), the peak position of tetragonal *004* shifted to a lower angle, and its relative intensity against tetragonal 400 increased under the electric field. A similar behavior was also observed for the films with a Zr/(Zr + Ti) ratio of 0.62, as shown in Fig. 6(b), even though the rhombohedral 400 peak coexisted. These results indicate the increase in the (001)-oriented domain as well as its elongation, irrespective of the existence of the rhombohedral domain. For that with a Zr/(Zr + Ti) ratio of 0.65, the asymmetric peak split into at least two peaks, as shown in Fig. 6(c), suggesting an increase in the fraction and lattice parameter of (100)-oriented tetragonal domain. The rhombohedral 400 peak asymmetrically broadened under the electric field for Zr/(Zr + Ti) ratio of 0.67, as shown in Fig. 6(d). This change is similar to that by the poling process for the film with Zr/(Zr + Ti) = 0.65 shown in Fig. 3(c).

The lattice parameters under the electric field estimated from the data shown in Fig. 6 are plotted in Fig. 5. The *c*-axis lattice parameter of the tetragonal phase increased under the electric field. The lattice parameter estimated from the lower angle peak of the film with Zr/(Zr + Ti) = 0.67 [see Fig. 6(d)] is on the extrapolated line of the *c*-axis lattice parameters (dash-dot line). These data suggest the possibility of a phase change from rhombohedral to tetragonal symmetry under an electric field for Zr/(Zr + Ti) = 0.67. Kovacova et al. reported a phase change from tetragonal to rhombohedral symmetry under an electric field for Zr/(Zr + Ti) = 0.5.[19] However, the phase change from rhombohedral to tetragonal symmetry is considered to be more reasonable because the polarization direction is parallel to the applied electric field. Observation of the polarization direction of the films by scanning probe microscopy and Raman scattering analysis is the next step of this study to determine constituent phases more precisely.

4. Conclusions

$Pb(Zr_xTi_{1-x})O_3$ films of approximately 1.5 μm thickness with various Zr/(Zr + Ti) ratios in the range 0.54–0.67 were prepared on $(100)_c SrRuO_3/(100)_c LaNiO_3/(111)Pt/TiO_2/SiO_2/Si$ substrates by pulse MOCVD. Single tetragonal phase, mixture of tetragonal and rhombohedral phases, and single rhombohedral phase were obtained for films with $Zr/(Zr + Ti) < 0.55$, $0.55 \leqslant Zr/(Zr + Ti) \leqslant 0.65$, and $Zr/(Zr + Ti) > 0.65$, respectively. All films show good ferroelectricity with similar P_r values, irrespective of the compositions and constituent phases of the as-deposited film. The poling treatment for the films, including tetragonal phase, increased the fraction of the (001)-oriented tetragonal domains. The (001)-oriented tetragonal domains increased even for films with Zr/(Zr + Ti) of 0.65, which consisted of a single rhombohedral phase. A further increase in the (001)-oriented tetragonal domains was observed for these films under an electric field, as well as the shift in the peak toward the lower angle. In addition, peak broadening was confirmed under an electric field for the rhombohedral film with a Zr/(Zr + Ti) ratio of 0.67, implying that the (001)-oriented tetragonal domain was present. These results suggest that both the poling treatment and biasing cause a phase change from the (100)-oriented rhombohedral to (001)-oriented tetragonal phases.

Acknowledgments

This work was supported by JSPS KAKENHI Grant Nos. 19K15288 and 26220907. We thank Mr. Mimura, Dr. Kodera and Dr. Ichinose for fruitful discussion.

ORCID iDs

Takao Shimizu https://orcid.org/0000-0001-9508-7601
Hiroshi Funakubo https://orcid.org/0000-0002-1106-200X

1) P. Muralt, J. Micromech. Microeng. **10**, 136 (2000).
2) V. Natarajan, E. Varadarajan, M. Rath, and J. Parui, Integr. Ferroelectr. **193**, 100 (2018).
3) N. Setter et al., J. Appl. Phys. **100**, 051606 (2006).
4) J. F. Scott and C. A. Paz de Araujo, Science **246**, 1400 (1989).
5) G. L. Smith et al., J. Am. Ceram. Soc. **95**, 1777 (2012).
6) P. Muralt and S. Trolier-Mckinstry, J. Electroceram. **12**, 7 (2004).
7) I. Kanno, H. Kotera, and K. Wasa, Sens. Actuators A **107**, 68 (2003).
8) C. B. Yeager and S. Trolier-McKinstry, J. Appl. Phys. **112**, 074107 (2012).
9) S. Hiboux, P. Muralt, and T. Maeder, J. Mater. Res. **14**, 4307 (1999).
10) B. Noheda, D. E. Cox, G. Shirane, J. A. Gonzalo, L. E. Cross, and S.-E. Park, Appl. Phys. Lett. **74**, 2059 (1999).
11) L. Fan, J. Chen, Y. Ren, and X. Xing, Inorg. Chem. **57**, 3002 (2018).
12) I. Baturin, N. Menou, V. Shur, C. Muller, D. Kuznetsov, J.-L. Hodeau, and A. Sternberg, Mater. Sci. Eng. B **120**, 141 (2005).
13) M. Wallace, R. L. Johnson-Wilke, G. Esteves, C. M. Fancher, R. H. T. Wilke, J. L. Jones, and S. Trolier-McKinstry, J. Appl. Phys. **117**, 054103 (2015).
14) S. Osone, Y. Shimojo, K. Brinkman, T. Iijima, and K. Saito, Appl. Phys. Lett. **90**, 262905 (2007).
15) P. Gerber, U. Böttger, and R. Waser, J. Appl. Phys. **100**, 124105 (2006).
16) Z.-X. Zhu, J.-F. Li, Y. Liu, and J. Li, Acta Mater. **57**, 4288 (2009).
17) N. Ledermann, P. Muralt, J. Baborowski, S. Gentil, K. Mukati, M. Cantoni, A. Seifert, and N. Setter, Sens. Actuators A **105**, 162 (2003).
18) T. Tsurumi, Y. Kumano, N. Ohashi, T. Takenaka, and O. Fukunaga, Jpn. J. Appl. Phys. 1 **36**, 5970 (1997).
19) V. Kovacova, N. Vaxelaire, G. Le Rhun, P. Gergaud, T. Schmitz-Kempen, and E. Defay, Phys. Rev. B **90**, 140101 (2014).
20) Y. K. Kim, H. Morioka, R. Ueno, S. Yokoyama, H. Funakubo, K. Lee, and S. Baik, Appl. Phys. Lett. **88**, 252904 (2006).
21) H. Kungl, R. Theissmann, M. Knapp, C. Baehtz, H. Fuess, S. Wagner, T. Fett, and M. J. Hoffmann, Acta Mater. **55**, 1849 (2007).
22) B. Noheda, Z. Zhong, D. E. Cox, G. Shirane, S.-E. Park, and P. Rehrig, Phys. Rev. B **65**, 3 (2002).
23) H. Fu and R. E. Cohen, Nature **403**, 281 (2000).
24) K. Nagashima, M. Aratani, and H. Funakubo, J. Appl. Phys. **89**, 4517 (2001).
25) M. Hinterstein, J. Rouquette, J. Haines, P. Papet, M. Knapp, J. Glaum, and H. Fuess, Phys. Rev. Lett. **107**, 077602 (2011).
26) S. Okamoto, S. Yokoyama, Y. Honda, G. Asano, and H. Funakubo, Jpn. J. Appl. Phys. **43**, 6567 (2004).
27) H. Morioka, K. Saito, T. Kobayashi, S. Yasui, T. Kurosawa, and H. Funakubo, Jpn. J. Appl. Phys. **48**, 09KA03 (2009).
28) S. Okamoto, P. S. S. R. Krishnan, S. Okamoto, S. Yokoyama, K. Akiyama, and H. Funakubo, Jpn. J. Appl. Phys. **56**, 10PF12 (2017).
29) C. M. Foster, G.-R. Bai, R. Csencsits, J. Vetrone, R. Jammy, L. A. Wills, E. Carr, and J. Amano, J. Appl. Phys. **81**, 2349 (1997).
30) M. Nakajima, S. Okamoto, H. Nakaki, T. Yamada, and H. Funakubo, J. Appl. Phys. **109**, 091601 (2011).